Design and Construction of a Microcontroller-Based Portable Defibrillator

Rafiuddin Syam [1], Muhammad Almas Prasadawinata [2], Vina Oktaviani[3]
[2,3] Department of Electronic Engineering, Universitas Negeri Jakarta
[1] Department of Automation Engineering Technology, Universitas Negeri Jakarta
[1] rafiuddin_syam@unj.ac.id, [2] baggorden39@gmail.com

[1]

***Abstract* —** heart disease remains one of the leading causes of mortality in Indonesia. A defibrillator is an electronic medical device engineered to deliver a high-voltage electric shock of short duration to the cardiac muscle of patients experiencing acute cardiac abnormalities. The primary objective of this apparatus is to function as a critical resuscitation tool that administers an electrical countershock to restore normal sinus rhythm in patients afflicted with ventricular fibrillation or other shockable tachyarrhythmias. The core component of a defibrillator is a capacitor, which serves to store electrical energy temporarily. Upon reaching a pre-set energy level, the capacitor is discharged, channeling the stored voltage to the patient. Furthermore, contemporary defibrillators incorporate advanced technology to regulate current and pulse duration to achieve a specified energy dosage, a methodology known as current-based defibrillation. This approach is crucial as it prevents the delivery of a low-energy shock to a patient with high transthoracic impedance and avoids administering an excessively high-energy shock to a patient with low impedance, thereby enhancing safety and efficacy.

This research was conducted utilizing the Research and Development (R&D) methodology established by Borg and Gall, encompassing four primary stages: research and information collecting, planning, developing a preliminary form of the product, and preliminary field testing. The findings demonstrate that the constructed system is capable of charging the capacitor utilizing a primary 12 VDC power source, boosted to 400 VDC via a step-up module, to achieve target energy levels of 20 J, 30 J, 40 J, 50 J, and 60 J. The results, obtained from three separate measurements for each energy level, yielded the following average performance metrics: for 20 J, an average voltage of 231.8 V with an error margin of 0.8% and a charging efficiency of 99.2%; for 30 J, an average voltage of 284.2 V with an error margin of 0.96% and an efficiency of 99.04%; for 40 J, an average voltage of 332.6 V with an error margin of 3.7% and an efficiency of 96.3%; for 50 J, an average voltage of 365.7 V with an error margin of 0.28% and an efficiency of 99.72%; and for 60 J, an average voltage of 373.6 V with an error margin of 12.6% and an efficiency of 87.4%.

In conclusion, this study successfully developed a system that charges a capacitor from a 12 VDC source to a boosted voltage of 400 VDC, facilitating the delivery of specified energy levels from 20 J to 60 J. The system exhibited high charging efficiency and minimal error margins for energy levels up to 50 J. However, a notable decrease in performance was observed at the 60 J setting, indicated by a significant increase in the error margin and a reduction in efficiency. The capacitor charging duration was found to range from 12 seconds for the 20 J setting to 60 seconds for the 60 J setting.

Index Terms — Defibrillator, Joule, Arduino MEGA2560, Heart, Energy, Capacitor.

I. Introduction

Cardiovascular disease remains a leading cause of mortality in Indonesia. According to data from the Indonesian Ministry of Health, the number of cardiovascular disease cases—primarily coronary heart disease, stroke, and heart failure—reached 25,508 cases among males and 24,507 cases among females in 2015. The estimated mortality rate due to cardiovascular diseases in Indonesia is presented in Fig. 1.

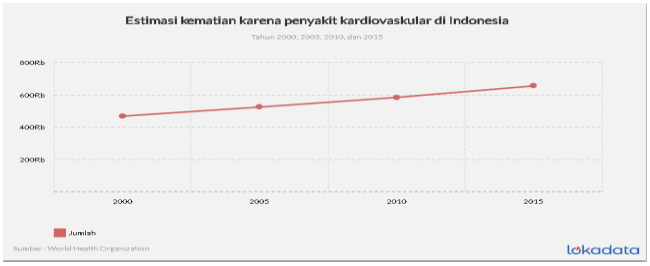

Fig. 1 Estimated deaths due to cardiovascular disease in Indonesia

One critical intervention to prevent mortality in cases of cardiac arrest is defibrillation, administered using a defibrillator, a significant technological advancement in medical equipment. Contemporary defibrillators employ current-based defibrillation technology, which regulates current and duration to deliver a specific energy dose (Dewi, 2017). This methodology prevents the delivery of low-energy shocks to patients with high impedance and avoids excessively high-energy shocks to patients with low impedance. Defibrillators are classified into two main types: biphasic and monophasic. For biphasic defibrillators, the recommended initial dose ranges from 120 to 200 joules. In contrast, monophasic defibrillators require a recommended dose of 360 joules (Goyal et al., 2022). The ECC Guidelines 2000 did not provide a definitive recommendation for the initial and subsequent energy levels for defibrillation attempts when using biphasic waveform devices

(Cummins, 2003). For pediatric patients, the recommended defibrillation dose is 2 J/kg. Subsequent doses may be increased to 4 J/kg, with a maximum dose of 10 J/kg. For each repeated defibrillation attempt, the administered dose must be at least equal to or higher than the previous dose (Goyal et al., 2022).

Research conducted by Arios (2020), entitled "Simulation of Energy Regulation in a Simple Defibrillator," resulted in the design of a basic defibrillator utilizing the main power grid (e.g., PLN) as its primary energy source. This study implemented energy settings at levels of 20J, 40J, 60J, 80J, and 100J, incorporating a discharge system to manage excess energy. However, the research by Arios (2020) had several limitations: it required a mains voltage power supply from the grid, utilized transistors as control signals for capacitor charging, stored capacitor energy on the electrodes, and managed energy discharge.

Based on the review of existing research, it is concluded that previous studies predominantly relied on the main power grid (PLN) as the primary energy source for activating the defibrillator. Furthermore, these designs typically produced an AC voltage on the paddles. To address these limitations, this study proposes the development of a device entitled "Design and Construction of an Arduino-Based Simple Defibrillator." This device utilizes a Li-Po battery as its power source and delivers a DC voltage to the paddles, thereby potentially reducing the risk of complications related to myocardial cell damage caused by high-energy shocks.

II. Basic Theory

A. Defibbrillator

According to Dabukke (2020), a defibrillator is an electronic device designed to deliver a high-intensity, short-duration electrical shock to the cardiac muscle of patients experiencing cardiac abnormalities. The primary purpose of this device is to serve as a life-saving tool that administers an electric countershock to normalize heart rhythm in patients suffering from ventricular fibrillation or other shockable abnormal rhythms. The defibrillator delivers a high-amplitude current impulse to the heart to restore normal rhythm and contractile function in patients experiencing ventricular fibrillation (VF) or pulseless ventricular tachycardia (VT).

Defibrillators are classified into two main types: biphasic and monophasic. For biphasic defibrillators, the recommended initial energy dose ranges from 120 to 200 joules. In contrast, monophasic defibrillators require a recommended dose of 360 joules (Goyal et al., 2022). The ECC Guidelines 2000 did not establish a definitive recommendation for the initial and subsequent energy levels for defibrillation attempts when using a biphasic waveform defibrillator (Cummins, 2003). For pediatric patients, the recommended defibrillation dose is 2 joules per kilogram. Subsequent doses may be increased to 4 joules per kilogram, with a maximum dose of 10 joules per kilogram. For each repeated defibrillation attempt, the administered dose must be at least equal to or higher than the previous dose (Goyal et al., 2022).

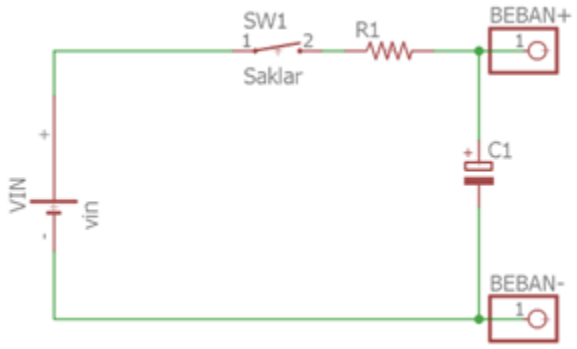

Fig. 2 RC circuit in defibrillator

The subsequent step is to transform the circuit equation into the frequency domain via the Laplace transform:

$$i = \frac{e_i - e_o}{R} \tag{2.1}$$

$$e_o = \frac{\int \quad i\,dt}{C} \tag{2.2}$$

The Laplace transformation of Equations 1 and 2, under zero initial conditions, becomes:

$$I(s) = \frac{E_i(s) - E_o(s)}{R} \tag{2.3}$$

$$E_o(s) = \frac{I(s)}{Cs} \tag{2.4}$$

Therefore, the block diagram corresponding to Equation 3 is as follows:

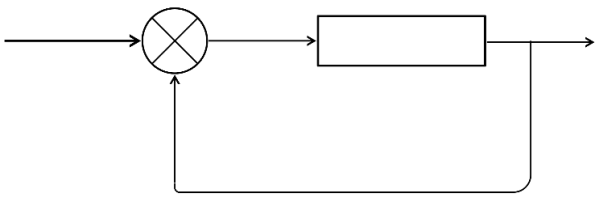

Fig. 3 block diagram shown in equation 3

PID control (proportional-integral-derivative) is implemented within a closed-loop system that incorporates feedback from the system output to achieve the desired response. The PID system regulates the input variable by manipulating the output variable, thereby generating a new input variable to ensure the system output conforms to specifications (Saka Gilap Asa et al., 2016). The combination of proportional control action, integral control action, and derivative control action is termed proportional-plus-integral-plus-derivative control action. The controller equation is expressed by the following formula (Ogata, 2017):

$$u(t) = K_p e(t) + \frac{K_p}{T_i}\int_0^t e(t)dt + K_p T_d \frac{de(t)}{dt} \tag{2.5}$$

or the transfer function is:

$$\frac{U(s)}{E(s)} = K_p\left(1 + \frac{1}{T_i s} + T_d s\right)$$

(2.6)

where K_p is the proportional gain, T_i is the integral time, and T_d is the derivative time. The block diagram of the proportional-integral-derivative controller is shown in Fig. 4 below.

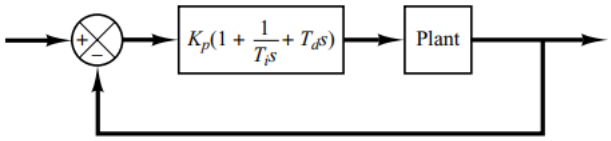

Fig. 4 PID Control System

So by combining the RC circuit block diagram with PID, the block diagram can be seen in Fig. 5.

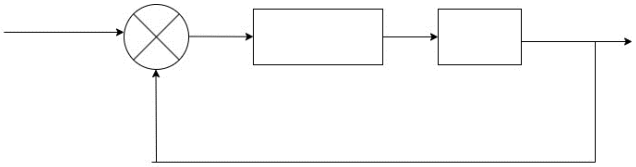

Fig. 5 PID Control System in RC Circuit

PID tuning using the Ziegler-Nichols method involves two distinct techniques. The first method utilizes two parameters, L (dead time) and T (time constant), which are derived from the process reaction curve (or S-shaped curve). These parameters are determined by drawing a tangent line at the inflection point of the curve and identifying its intersections with the time axis and the steady-state value line, c(t)=K. The values of L and T are then used to calculate the proportional gain (Kp), integral gain (Ki), and derivative gain (Kd).

The second method, often referred to as the ultimate cycle method, also requires two parameters: the ultimate gain (Ku) and the ultimate period (Tu). Ku is the critical value of the proportional gain at which the system output exhibits sustained oscillations. Tu is the period of these oscillations, measured in seconds as the time between successive peaks (Diah Ika Putri et al., 2022).

Ziegler and Nichols proposed rules for calculating the proportional gain, integral time, and derivative time based on these empirically determined plant characteristics. This approach enabled field engineers to perform plant experiments to determine the parameters for PID controller tuning. (Since the original Ziegler-Nichols proposal, numerous other PID tuning rules have been developed, as documented in the literature and by controller manufacturers) (Ogata, 2017).

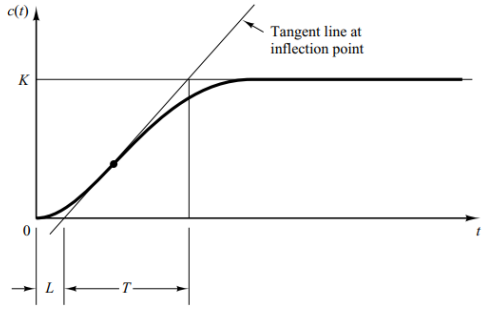

Fig. 6 Respondents are in the shape of an S curve.

Type of Controller	K_p	T_i	T_d
P	$\frac{T}{L}$	∞	0
PI	$0.9\frac{T}{L}$	$\frac{L}{0.3}$	0
PID	$1.2\frac{T}{L}$	$2L$	$0.5L$

Fig. 7 Kp, Ti, and Td values based on L and T parameters

The function C(s)/U(s) can be approximated by a first-order system with the equation:

$$\frac{C(s)}{U(s)} = \frac{Ke^{-Ls}}{Ts+1} \tag{2.7}$$

Ziegler and Nichols proposed specific formulas to determine the values of KpKp, TiTi, and TdTd. When configuring the PID controller using the first method of the Ziegler-Nichols rules, the following relationships are applied:

$$\begin{aligned} G_c(s) &= K_p\left(1 + \frac{1}{T_i s} + T_d s\right) \\ &= 1.2\frac{T}{L}\left(1 + \frac{1}{2Ls} + 0{,}5Ls\right) \\ &= 0.6T\frac{\left(s + \frac{1}{L}\right)^2}{s} \end{aligned} \tag{2.8}$$

B. Hardware

Hardware design is conducted to determine the hardware components that will be utilized in the research. This process ensures that the system to be developed is well-directed and can be confirmed to function correctly. The hardware components employed in this study are as follows:

The Arduino Mega 2560 is a microcontroller board based on the ATmega2560 chip. It features 54 digital input/output pins, of which 15 can be used as PWM outputs, 16 as analog inputs, and 4 as UARTs (hardware serial ports). The board is equipped with a 16 MHz crystal oscillator, a USB connection, a power jack, an ICSP header, and a reset button. These components provide all the necessary support for the microcontroller. The board can be powered and activated simply by connecting it to a computer via a USB cable or to an

AC-DC adapter or battery. The Arduino Mega 2560 is compatible with most shields designed for the Arduino Duemilanove or Diecimila boards. It represents the latest version, superseding the previous Arduino Mega (MAJID, 2016).

Fig. 8 Arduino MEGA 2560

The subsequent component is the capacitor. According to (Dwi Astuti, 2019), a capacitor is an electronic component used to store electric charge. It consists of two conductor plates (often made of silver or aluminum) separated by a dielectric medium (such as ceramic or porcelain).

The functions of a capacitor are as follows:

1. To temporarily store electric charge and energy.
2. To select frequencies in radio receivers (frequency tuning).
3. To act as a filter in power supply circuits.
4. To block direct current (DC), thereby preventing DC from passing through the capacitor.

The selection of a capacitor within a circuit is dependent on its energy storage capacity. The energy stored in a capacitor is equivalent to the work performed during the charging process. When the capacitor is discharged, this stored energy accounts for the work done by the electric force (Siagian, 2020).

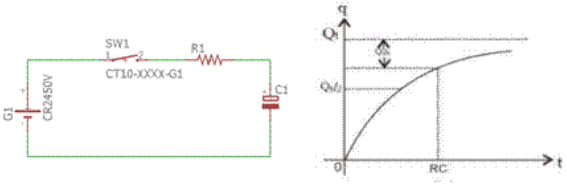

Fig. 9 Capacitor Charging

During the capacitor charging process, the potential difference across points bc (V_bc) increases, while the potential difference across points ab (V_ab) across the resistor decreases, corresponding to the decrease in current. The sum of these two potential differences remains constant and is equal to the electromotive force (ε) of the battery. After a certain period, the capacitor becomes fully charged, the current in the circuit decays to zero, and the potential difference across the resistor also becomes zero. Consequently, the entire source voltage of the battery is present across the capacitor, and V_c = ε. These potential differences can be expressed by the following equations:

$$V_{ab} = iR \tag{2.9}$$

We can find it in this way

$$i = \frac{\varepsilon}{R} - \frac{q}{RC} \tag{2.10}$$

We can obtain a general form for charge and current as a function of time. By choosing the positive direction of the current to have the same value as the positive charge of the capacitor plate (the current is towards the positive plate of the capacitor), we obtain the following equation:

$$\frac{dq}{q - C\varepsilon} = \frac{dt}{RC} \tag{2.11}$$

So we can find out in a way

$$q = C\varepsilon(1 - e^{-\frac{t}{RC}}) \tag{2.12}$$

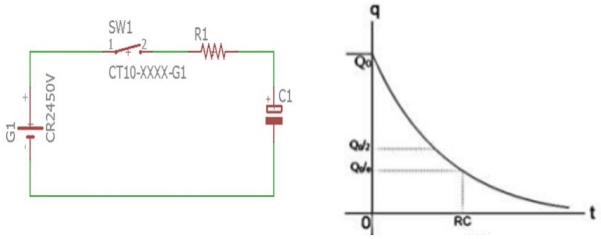

Fig. 10 Capacitor Discharge

As with charging, we call and the current and charge time-dependent immediately after the connection is made. Then we use Kirchoff's loop rule with , so that:

$$i = \frac{dq}{dt} = -\frac{q}{RC} \tag{2.13}$$

After the capacitor is fully charged and the voltage source is disconnected, the electric charge on the capacitor will not dissipate instantaneously. Instead, a finite amount of time is required for the capacitor to discharge completely.

The absolute value of the charge on each capacitor plate is denoted as qq. When the capacitor is charged, the two plates hold charges of equal magnitude but opposite sign: +q+q and −q−q. It is important to note that the net charge of the entire capacitor remains zero, and is not equal to qq. Every point on a single plate is at the same electric potential because the plate is a conductor. For a capacitor, the charge qq and the potential difference VV between the plates are proportional to each other, as given by the equation:

$$q = CV \tag{2.14}$$

Suppose a charge qq has been transferred from one capacitor plate to the other, resulting in a potential difference V=q/CV=q/C between the plates. If an additional infinitesimal charge dqdq is then transferred, the work done in this process is stored in the capacitor as potential energy dUdU. This relationship is expressed by the differential equation:

$$U = \frac{q^2}{2C}$$

(2.15)

From Equation 3, we can write as follows:

$$U = \frac{1}{2} xCV^2$$

(2.16)

The next component is the diode. A diode is a fundamental component in electronic devices such as solar cells and photodetectors. The most critical property of a diode for solar cell applications is its photoconductive nature, which refers to the magnitude of the current generated when the diode absorbs photons from incident light. Based on their active material composition, there are two primary types of diodes: the p-n junction diode and the Schottky diode (Setya, 2017).

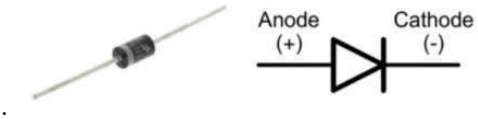

Fig. 11 Rectifier Diode

The next component is the Lithium-Polymer (Li-Po) battery. A Li-Po battery is a newer type of battery that is widely used in numerous electronic devices. It has become a primary choice for consumers who require high power output and long operational duration (Joko et al., 2017). A Li-Po battery cell has a nominal voltage of 3.7 V. Therefore, a battery comprising three cells in series yields a total nominal voltage of 11.1 V. When fully charged, the voltage per cell reaches approximately 4.2 V. The minimum safe voltage threshold for initiating a charging cycle is 3.0 V per cell; if the cell voltage falls below this level, the battery is likely to have sustained damage.

Fig. 12 Li-Po battery

The next component is the Capacitor Charging Driver. A capacitor charging driver is a type of buck-boost DC-DC converter. According to (Kurniawan, 2018), in a buck-boost converter, the stability of the output voltage is determined by the performance of its boost section. In a boost converter, fluctuations in the output voltage cannot be directly mitigated by simply increasing or decreasing the switch-on/off time or the duty cycle of the switching pulse. To respond rapidly to load variations, boost converters typically employ multiple operational modes. However, transitions between these operational modes can disrupt the stability of the output voltage.

Furthermore, (Kurniawan, 2018) categorizes soft-switching techniques into two types: Zero Voltage Switching (ZVS) and Zero Current Switching (ZCS). ZVS ensures the voltage across the electronic switching component is conditioned to be zero before the current begins to rise. Conversely, ZCS ensures the current through the electronic switching component is conditioned to be zero before the voltage begins to rise. The function of the capacitor charging driver is to charge the capacitor via a step-up process.

TABLE 1
ZVS converter charger capacitor driver specifications

Input tegangan	8– 32 VDC
Input Arus	5 A(Max)
Output tegangan	+45V-390V
Output arus	0,2 A (Max)
Output Power	40 W (peak 70 W)
Kerja Temperatur	40 – 85 ℃
Operator Frekuensi	75 KHz

Fig. 13 Charging Capacitor Driver

The next component is the Relay Module. A relay is an electronic component that functions as a switch; specifically, it operates as an electrically actuated mechanical switch. Relays utilize an electromagnetic force to open or close their contacts. They are employed to control a large current or voltage circuit using a significantly smaller control current or voltage. Furthermore, relays can function as control logic elements within a system (Eddi Kurniawan, 2013).

Fig. 14 1 Channel Relay Module

The subsequent component is the 20x4 Liquid Crystal Display (LCD). An LCD is an interface medium used to present the output data from an electronic circuit (Saputra, 2020). These displays are typically available as integrated modules featuring dedicated pins for data communication, power supply control, and display contrast adjustment.

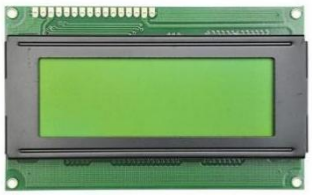

Fig. 15 LCD (Liquid Crystal Display) 20x4

III. METHODOLOGY

This research was conducted using the Research and Development (R&D) method by Borg and Gall, which encompasses four main stages: (1) research and information collection, (2) planning, (3) development of a preliminary product form, and (4) preliminary field testing.

A. Software Applications

Following the hardware design phase utilizing the specified components, software is required to program the control system to ensure it functions according to the intended design. The programming was carried out using the Arduino IDE and MATLAB software. The software tools employed are as follows:

1. Arduino IDE

   The Arduino IDE utilizes the C/C++ programming language. The Arduino Integrated Development Environment (IDE) is an application that incorporates an editor, compiler, and uploader, and is compatible with all modules in the Arduino family series, such as the Arduino Duemilanove, Uno, Bluetooth, Mega, and Nano. Exceptions include certain Arduino-produced boards that utilize microcontrollers outside the AVR series, such as those based on ARM microprocessors. The sketch editor within the Arduino IDE supports features such as line numbering and syntax highlighting, which facilitates syntactic code checking (PANDIANGAN, 2019).

B. Design Defibrilator

Following the completion of the hardware and software design phases, this research proceeded to the device design stage. The resulting design can be observed in Figure 16 below.

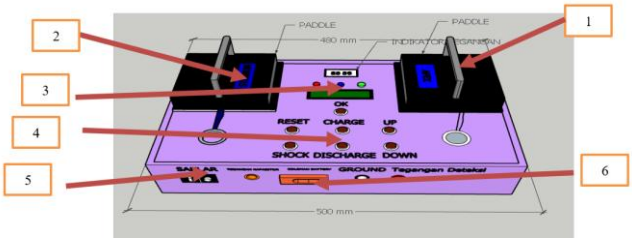

Fig. 16 Defibrillator Design

The components of this portable defibrillator can be seen in Figure 16 below as follows:

1. The apex paddle functions to deliver a positive electrical charge to the patient's body.
2. The sternum paddle functions to deliver a negative electrical charge to the patient's body.
3. The 20x4 LCD screen functions to display the energy joule settings, shock, charge, and discharge status.
4. The push button functions to navigate and select menus on the device.
5. The switch functions to activate or disconnect the device's power source.
6. The battery connector functions to power the device.

C. Block Diagram of Tool Work

Based on the block diagram above, the function of each system block can be explained, demonstrating the initial stages in designing a Portable Defibrillator device based on a Microcontroller.

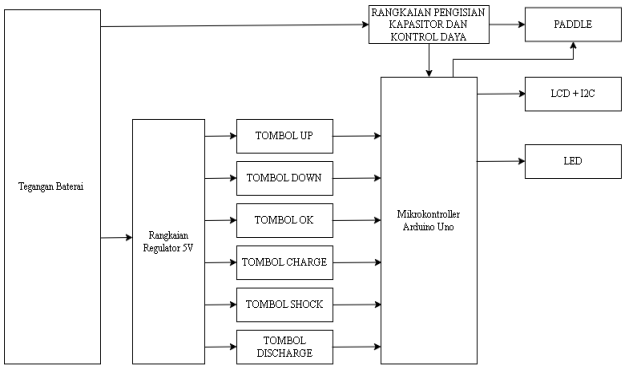

Fig. 17 Block Diagrams

D. *Tool Work Flowchart*

The flowchart of the designed system begins when the power switch is turned on, which activates the LCD display as an indicator of the device's operational status. The output section includes an LCD component that displays system parameters, specifically a voltage (V) reading of 400 VDC and an initial current (I) of 70 mA. The subsequent component involves setting the target output energy via the "energy setting" interface. In this stage, the operator can adjust the energy level to be delivered by the paddles, selecting values within the range of 20 to 60 Joules.

The "charge" button initiates the capacitor charging process. Once activated, the system enters the charging phase, during which the capacitor is charged to the predetermined energy level. Upon completion of the charging process, the next step involves delivering the stored capacitor voltage to the respective paddles—apex and sternum—by pressing the "shock" button, thereby administering the therapeutic shock to the patient. If an energy setting error occurs, the capacitor can be discharged by pressing the "discharge" button. After discharging, the energy setting process can be repeated anew.

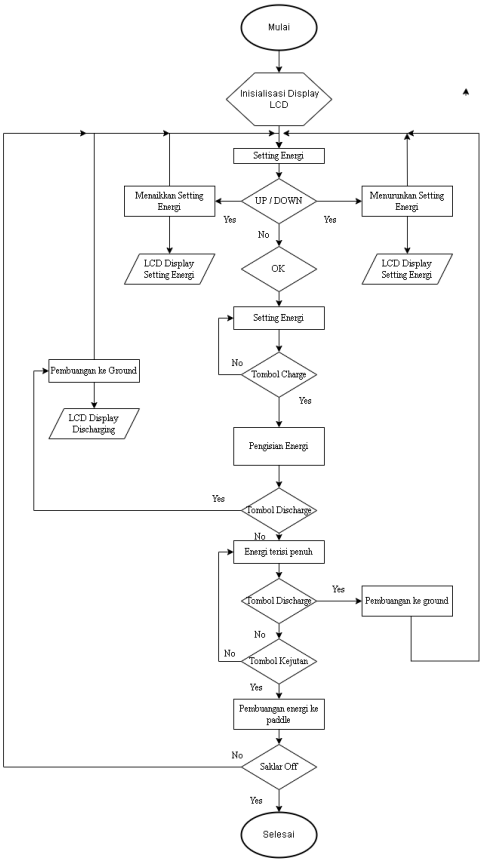

Fig. 18 Tool Work Flowchart

IV. Results and Analysis

A. Description of Research Results

Based on the block diagram and flowchart developed and discussed in the previous section, the researcher will evaluate the design results of the microcontroller-based portable defibrillator. The researcher will conduct testing according to the methodology outlined in the previous chapter. Subsequently, the researcher will describe the testing results and the design of the device. The physical implementation of the device can be observed in Fig. 19 below.

Fig. 19 Overall Portable Defibrillator Results

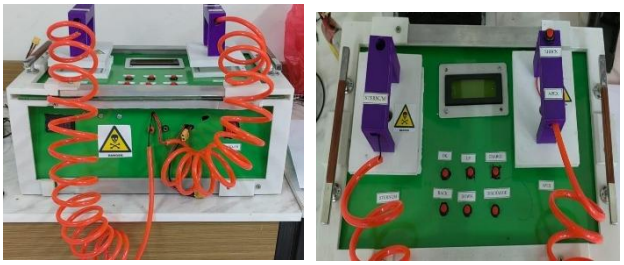

Fig. 20 Top view and side view of the Defibrillator

The components of this portable defibrillator can be observed in Fig. 21 below, with the following descriptions:

1. The Arduino Mega 2560 PCB Shield functions as the central control unit of the device.
2. The 1-channel relay module functions to connect or disconnect the electrical voltage and current to the input of the step-up module.
3. The 2-channel relay module functions to control the main relay for capacitor charging and discharging.
4. The 5600 Ohm resistor functions as a component for capacitor discharging.
5. The Bosch relay functions to connect or disconnect the voltage and current during capacitor charging.
6. The 5600 Ohm resistor functions as a component for capacitor charging.
7. The Bosch relay functions to connect or disconnect the main voltage and current in the capacitor control circuit.
8. The resistor functions as a voltage divider.
9. The 750 µF capacitor functions to temporarily store electrical charge.

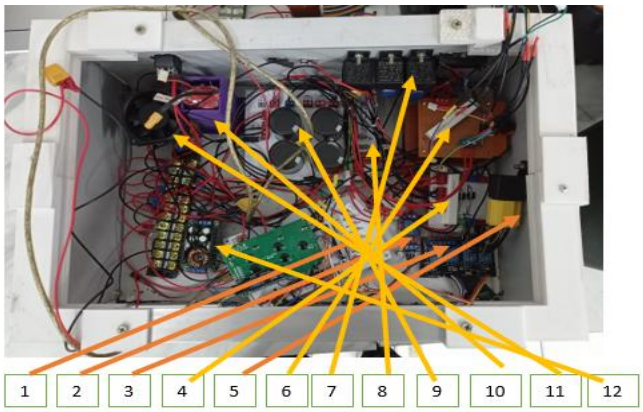

Fig. 21 Parts of a Portable Defibrillator

B. Discussion of Test Results

Based on the conducted testing, the microcontroller-based portable defibrillator system is designed to deliver electrical energy utilizing an initial voltage boosted through a step-up module circuit. This research employed the Research and Development (R&D) method, which was carried out in four stages: (1) data collection and design planning, as elaborated in Chapter 2; (2) development phase, as detailed in Chapter 3; and (3) the final testing phase, which is discussed in this chapter (Chapter 4) to evaluate the research outcomes. The portable defibrillator prototype was designed to configure energy levels using voltage as the reference parameter. The system utilizes an

Arduino Mega 2560 as the microcontroller and is powered by a Li-Po battery.

Furthermore, the functionality and performance of the device were validated by comparing the hardware test results against the predetermined design criteria.

1. Calculation of Capacitor Energy Size

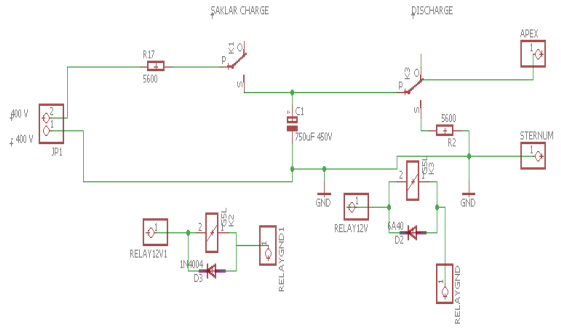

Fig. 22 Capacitor Control Circuit

In the case example shown in Figure 13, the capacitor charging voltage required to achieve the specified energy levels is as follows: **U_1 = 20 J, U_2 = 30 J, U_3 = 30 J, U_4 = 40 J, U_5 = 50 J, and U_6 = 60 J**, using Equation 8 as derived below.

For instance, to determine the voltage for U_1 = 20 J, the capacitor voltage is calculated as follows:

$$U_1 = \frac{1}{2}\, x750x10^{-6}\, x\, E^2$$

$$E = 230\, V$$

Using the same method, the required voltages for the other energy levels are obtained as shown below.

No	Work Output (Joules)	Voltage output (V)
1	U_1	230
2	U_2	282
3	U_3	326
4	U_4	365
5	U_5	400

a) Calculation of Capacitor Charging Time

The time required to charge the capacitor to the specified voltages—Vc_1 = 230.9 V, Vc_2 = 282.8 V, Vc_3 = 326.5 V, Vc_4 = 326.5 V, Vc_5 = 365.1 V, and Vc_6 = 400 V—is determined using Equation 9, as outlined below.

For example, the time required to charge the capacitor to Vc_1 = 230.9 V is calculated as follows:

$$V_{c_1} = \frac{q}{c} = E\left(1 - e^{-\frac{t_1}{RC}}\right)$$

$$30{,}9\, V = 400\left(1 - e^{\frac{t}{5600\, x\, 0{,}00075}}\right)$$

$$t = 3{,}61\, s$$

So in the same way it is obtained as below.

No	Voltage Output (V)	Time (s)
1	V_{c_1}	3,61
2	V_{c_2}	5,14
3	V_{c_3}	7,11
4	V_{c_4}	10,24
5	V_{c_5}	13,79

2. Control System in RC Circuits

To construct a block diagram of a system, the first step is to formulate equations that describe the dynamic behavior of each individual component. Subsequently, the Laplace transform of these equations is derived, as expressed by the following relationship:

$$\mathrm{i} = \frac{e_i - e_o}{R}$$

$$e_o = \frac{\int\ i\, dt}{C}$$

The Laplace transform of the aforementioned equations, under zero initial conditions, is expressed as follows:

$$\mathrm{I(s)} = \frac{E_i(s) - E_o(s)}{R}$$

$$E_o(s) = \frac{I(s)}{Cs}$$

Therefore, the simplification performed is as follows:

$$= \frac{\frac{1}{RCS}}{1+\frac{1}{RCS}}$$

$$= \frac{1}{RCS+\frac{RCS}{RCS}}$$

$$= \frac{1}{1+RCS}$$

Therefore, the block diagram representation of the transfer function is as follows:

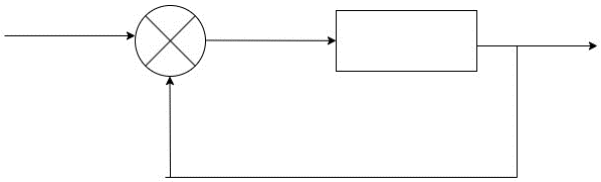

Fig. 23 Block diagram of RC Circuit of Control Engineering System

$\mathrm{H(s)} = \frac{E_O(s)}{E_i(s)} = \frac{1}{1+\,RCS}$, then the results obtained

$\mathrm{H(s)} = \frac{E_O(s)}{E_i(s)} = \frac{1}{1+\,5600\, x\, 0{,}00075S}$

$\mathrm{H(s)} = \frac{1}{1+\,4{,}2S}$

Therefore, the graphical representation of the step response generated using MATLAB software can be observed in Fig. 24 below:

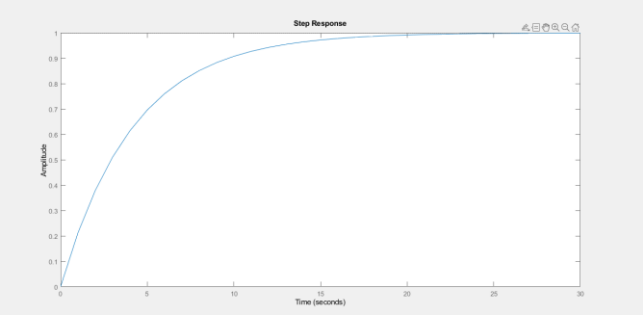

Fig. 24 Step Response Graph of RC Circuit

C. PID Simulation Calculation

1. Trial and Error Testing

In this test, the author implemented the PID controller parameters (Kp, Ki, and Kd) using a trial-and-error method. The transfer function model of the RC circuit used was:

$$H(s) = \frac{1}{1+4,2S}$$

In this test, the PID controller parameters (Kp, Ki, and Kd) were implemented using a trial-and-error method, with the transfer function model of the RC circuit serving as the basis for simulation in MATLAB software. Three distinct cases were evaluated: the first case employed values of Kp = 0.5, Ki = 0.2, and Kd = 0.1, resulting in an overshoot of 2%; the second case utilized Kp = 0.5, Ki = 0.2, and Kd = 0.2, also yielding an overshoot of 2%; and the third case applied Kp = 0.5, Ki = 0.2, and Kd = 0.5, with the corresponding output response detailed graphically. The simulation results for all cases are presented in Fig. 25.

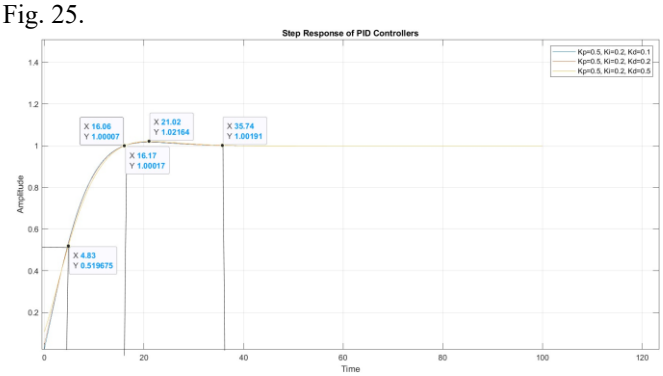

Fig. 25 Step Response RC Circuit with PID control using Trial and Error method

Kp, Ki and Kd values	Down Time (T_s)	Ride Time (T_r)	Delay Time (T_d)	Peak Times (T_d)	Maximum Overshoot (M_p)
Kp = 0,5 Ki = 0,2 Kd = 0,1	35,74	16,06	4,83	33	1.017
Kp = 0,5 Ki = 0,2 Kd = 0,2	35,74	16,06	4,83	34	1,017
Kp = 0,5 Ki = 0,2 Kd = 0,5	35,74	16,17	4,83	36	1,021

Using a trial-and-error approach for PID controller tuning across three distinct cases with varying values of Kp, Ki, and Kd, the following results were observed. In the first case, with parameters set to Kp = 0.5, Ki = 0.2, and Kd = 0.1, the system exhibited a settling time (T_s) of 35.74 seconds, a rise time (T_r) of 16.06 seconds, a delay time (T_d) of 4.83 seconds, a peak time (T_p) of 33 seconds, and a maximum overshoot (M_p) of 1.017. For the second case, utilizing values of Kp = 0.5, Ki = 0.2, and Kd = 0.2, the performance metrics remained largely consistent, with a settling time (T_s) of 35.74 seconds, a rise time (T_r) of 16.06 seconds, a delay time (T_d) of 4.83 seconds, a peak time (T_p) of 34 seconds, and a maximum overshoot (M_p) of 1.017. In the third case, with parameters Kp = 0.5, Ki = 0.2, and Kd = 0.5, the system demonstrated a settling time (T_s) of 35.74 seconds, a rise time (T_r) of 16.17 seconds, a delay time (T_d) of 4.83 seconds, a peak time (T_p) of 36 seconds, and a maximum overshoot (M_p) of 1.021. These results indicate that while the settling and delay times remained stable across all cases, variations in the derivative gain (Kd) influenced the rise time, peak time, and overshoot, albeit marginally.

2. Results of the Ziegler Nichols method test

In this method, the authors constructed an S-curve and identified the intersection points to determine the values of the delay time (L) and time constant (T). This testing approach utilized the same transfer function model as the previous method. The resulting curve, with intersection lines used to measure the delay time (L) and time constant (T), is presented in Fig. 26.

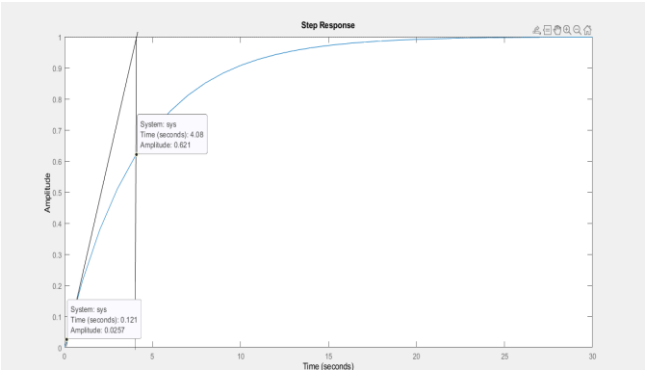

Fig. 26 Step Response determines L and T

Based on Figure 26, the obtained values are L = 0.01, T = 4, and K = 1. Consequently, the formula applied in the equation is as follows:

$$\frac{U(s)}{E(s)} = K_p\left(1 + \frac{1}{T_i s} + T_d s\right)$$

So the results obtained are:

$$= \frac{U(s)}{E(s)} = K_p\left(1 + \frac{1}{T_i s} + T_d s\right)$$

$$= \frac{U(s)}{E(s)} = 1.2\frac{T}{L}\left(1 + \frac{1}{2Ls} + 0{,}5Ls\right)$$

$$= \frac{U(s)}{E(s)} = 1.2\frac{4}{0{,}01}\left(1 + \frac{1}{2x0{,}01s} + 0{,}5x0{,}01s\right)$$

This test utilized MATLAB software to simulate the PID control response using the Ziegler-Nichols method. Three distinct cases were evaluated: the first case employed parameters Kp = 40, Ki = 167.19, and Kd = 2.5, resulting in an overshoot of 14%; the second case used Kp = 16.3, Ki = 27.2, and Kd = 2.45, yielding an overshoot of 12%; and the third case applied Kp = 30, Ki = 75, and Kd = 3, achieving an overshoot of 11%. The graphical results of these simulations are presented in Figure 27.

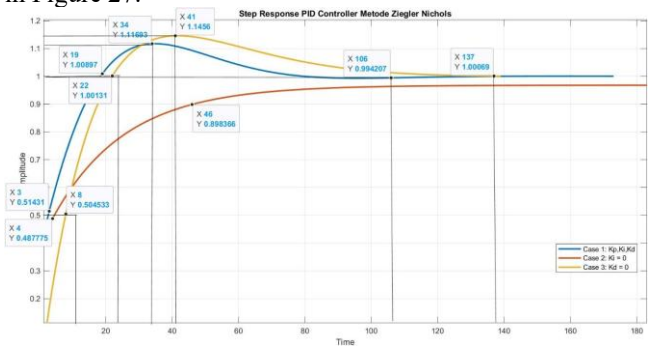

Fig. 27 PID Step Response using Ziegler Nichols method

Delay Time (L)	Time Constant (T)	Kp, Ki and Kd values	Down time (T_s)	Ride Time (T_r)	Delay Time (T_d)	Peak Times (T_p)	Maximum Overshoot (M_p)
0,2	5,0	Kp = 30 Ki = 75 Kd = 3	106	19	3	34	1.11
0,2	5,0	Kp = 30 Ki = 0 Kd = 75	0	46	4	0	0
0,2	5,0	Kp =30 Ki = 75 Kd = 0	137	22	8	41	1,14

Using the Ziegler-Nichols method for PID controller tuning across three cases with different values of Kp, Ki, and Kd, the following results were observed. In the first case, with parameters Kp = 30, Ki = 75, and Kd = 3, the system exhibited a settling time (T_s) of 106 seconds, a rise time (T_r) of 19 seconds, a delay time (T_d) of 3 seconds, a peak time (T_p) of 34 seconds, and a maximum overshoot (M_p) of 1.11. For the second case, with parameters Kp = 30, Ki = 0, and Kd = 3, the performance metrics showed a settling time (T_s) of 0 seconds, a rise time (T_r) of 46 seconds, a delay time (T_d) of 4 seconds, a peak time (T_p) of 0 seconds, and no overshoot (M_p = 0). In the third case, with parameters Kp = 30, Ki = 75, and Kd = 0, the system demonstrated a settling time (T_s) of 137 seconds, a rise time (T_r) of 22 seconds, a delay time (T_d) of 8 seconds, a peak time (T_p) of 41 seconds, and a maximum overshoot (M_p) of 1.14. These results highlight the significant impact of integral and derivative gains on system dynamics, particularly in terms of overshoot, settling time, and transient response characteristics.

D. Capacitor Voltage Test Results

The comparative results between calculated measurements and those obtained using an Avometer (multimeter), derived from the average of three experimental trials, are presented in Table 1. This comparison illustrates the alignment between theoretical voltage values and empirical measurements taken with the Avometer.

Energy (Joules)	Measurement by calculation (Volt)			Measurement using Avometer (Volt)			Average Error	Charging Efficiency
	I	II	III	I	II	III		
20 J	230,9 V	230,9 V	230,9 V	233,4 V	231 V	231,3 V	0,8%	99,2%
30 J	282,8 V	282,8 V	282,8 V	284,4 V	284,9 V	283,4 V	0,96%	99,04 %
40 J	326,5 V	326,5 V	326,5 V	331,1 V	332,8 V	333,9 V	3,7%	96,3%
50 J	365,1 V	365,1 V	365,1 V	366 V	365,6 V	365,5 V	0,28%	99,72 %
60 J	400 V	400 V	400 V	354 V	383 V	383,8 V	12,6%	87,4%

The comparative graph of the capacitor voltage, illustrating both theoretical values and measurements obtained using an Avometer, is presented in Figure 28 below.

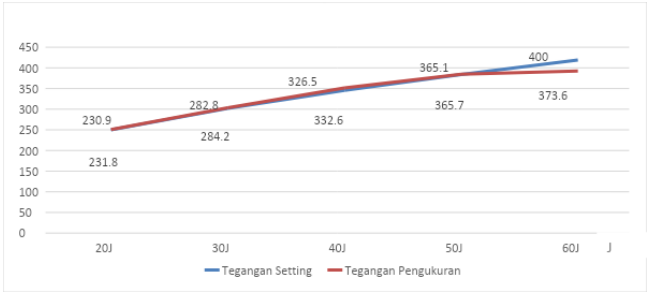

Fig. 28 Capacitor Voltage Test Results Graph

The test results indicate that the capacitor voltage achieved an average minimum of 231.8 V for 20 J and a maximum of 373.6 V for 100 J, with a minimal error margin of 0.8% corresponding to a charging efficiency of 99.2%, and a maximal error margin of 12.6% corresponding to a charging efficiency of 87.4%.

E. Energy Test Results

The capacitor energy test was conducted to evaluate the performance outcomes, as measured using a defibrillator analyzer. The results are summarized in the graph presented in Fig. 29 below.

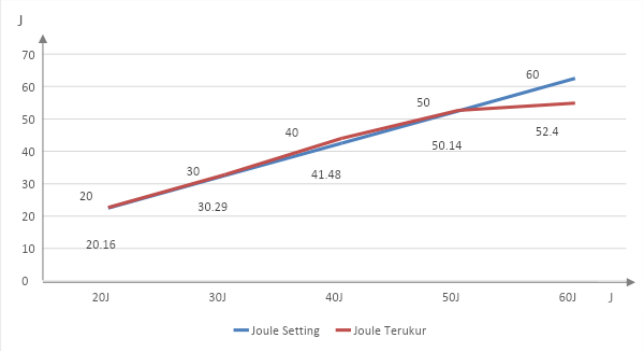

Fig. 29 Energy Test Results

The test results were accurately interpreted using the defibrillator analyzer, revealing that the measured energy output ranged from a minimum of 23 J (compared to the target 20 J) to a maximum of 59 J (compared to the target 60 J).

F. Capacitor Charging Time Test Results

The capacitor charging time test was conducted to determine the duration required for the capacitor charging process. The results of the capacitor charging time measurements are summarized in Table 2 below:

TABLE 2
Test results for charging time of 20 Joule capacitor

No.	Time (second)	Voltage out (Volt)		
		I	II	III
1.	0	0,6 V	0,2 V	1,7 V
2	3	68,3 V	63,9 V	70,8 V
3	6	128,9 V	125,2 V	130,7 V
4	9	177,4 V	174,4 V	178,9 V
5	12	220,1 V	217,5 V	221,2 V

The graph illustrating the time required to charge the capacitor to achieve a voltage corresponding to 20 J of energy is presented in Fig. 30 below.

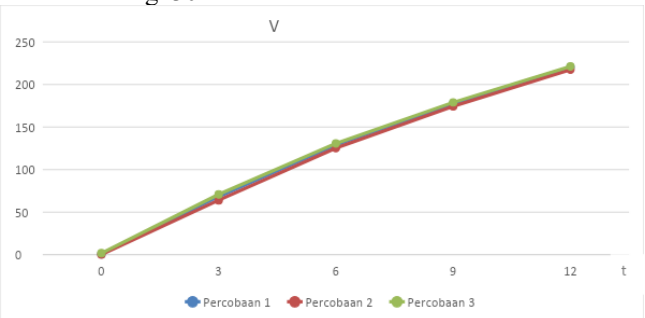

Fig. 30 Test results of the charging time of a 20 Joule capacitor

TABLE 3
Test results for charging time of 30 Joule capacitor

No.	Time (second)	Voltage out (V)		
		I	II	III
1.	0	0,8 V	1,1 V	1,5 V
2	3	63,8 V	63,6 V	65,8 V
3	6	125,2 V	130,5 V	132,1 V
4	9	174,5 V	183 V	184,3 V
5	12	214,2 V	214,1 V	215,2 V
6	15	245,7 V	249,6 V	247,6 V
7	18	275,5 V	278,1 V	278,9 V

The graph depicting the time required to charge the capacitor to the voltage level corresponding to 20 J of energy is shown in Fig. 22 below.

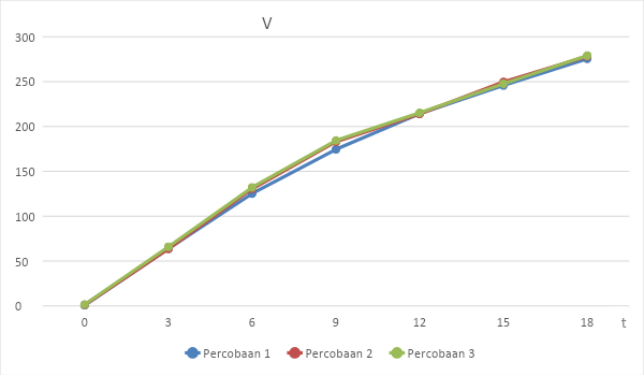

Fig. 31 Test results of the charging time of a 30 Joule capacitor

TABLE 4
Test results for charging time of 40 Joule capacitor

No.	Time (second)	Voltage out (V)		
		I	II	III
1.	0	1,0 V	0,5 V	1,8 V
2	3	60,8 V	65,3 V	70,1 V
3	6	128,3 V	126,3 V	130,2 V
4	9	176,9 V	179,7 V	182,8 V
5	12	216,2 V	221,9 V	224,5 V
6	15	251,2 V	250,2 V	255,3 V
7	18	276,9 V	278,5 V	280 V

8	21	297,7 V	299,4 V	302,9 V
9	24	313,6 V	315,6 V	315,6 V

The graph depicting the time required to charge the capacitor to the voltage level corresponding to 20 J of energy is presented in Figure 32 below.

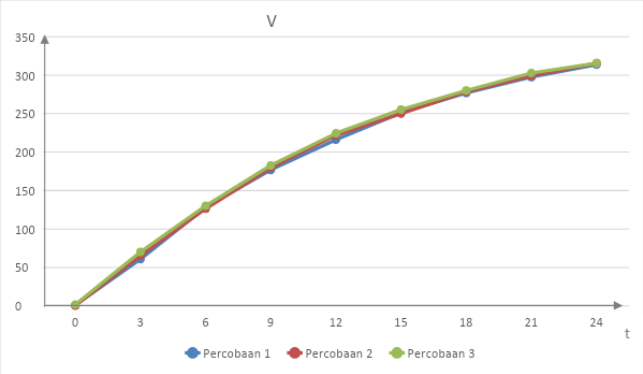

Fig. 32 Test results of the charging time of a 40 Joule capacitor

TABLE 5
Test results for charging time of 50 Joule capacitor

No.	Time (second)	Voltage out (V)		
		I	II	III
1.	0	0,1 V	1,2 V	1,3 V
2	3	54 V	71 V	71,4 V
3	6	116 V	130,9 V	131,2 V
4	9	167 V	183,3 V	183,6 V
5	12	208 V	221,3 V	221,6 V
6	15	245 V	252,5 V	252,9 V
7	18	271 V	280,3 V	278,5 V
8	21	293 V	300,8 V	303,2 V
9	24	312 V	315,2 V	315,4 V
10	27	326 V	330,5 V	331,4 V
11	30	339 V	340,6 V	342,7 V
12	33	348 V	351,3 V	352 V
13	36	354 V	358,1 V	359,1 V

The graph illustrating the time required to charge the capacitor to the voltage corresponding to 50 J of energy is presented in Figure 33 below.

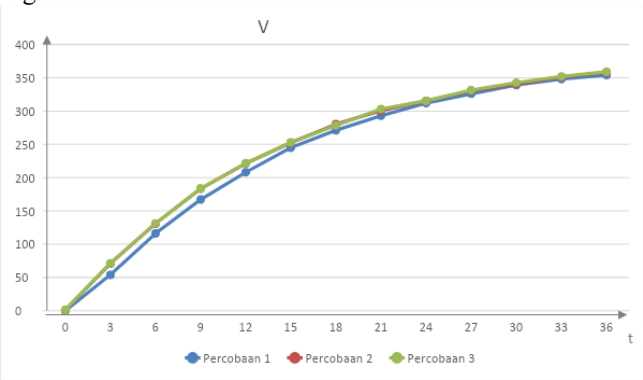

Fig. 33 Test results of the charging time of a 50 Joule capacitor

TABLE 6
Test results for charging time of 60 Joule capacitor

No.	Time (second)	Voltage out (V)		
		I	II	III
1.	0	0,2 V	0,7 V	0,8 V
2	3	44 V	63,2 V	63,9 V
3	6	121 V	124,7 V	125,2 V
4	9	161 V	174 V	174,5 V
5	12	203 V	217,3 V	217,7 V
6	15	241 V	249,3 V	249,7 V
7	18	268 V	275,5 V	275,8 V
8	21	291 V	300,8 V	299,2 V
9	24	309 V	313,7 V	314,1 V
10	27	327 V	328,2 V	328,6 V
11	30	337 V	340,1 V	341,6 V
12	33	341 V	349,7 V	350,2 V
13	36	358 V	358,7 V	358,8 V
14	39	364 V	365,6 V	365,5 V
15	42	366 V	369,7 V	370,3 V
16	45	370 V	373 V	374,1 V
17	48	372 V	375,9 V	377,5 V
18	51	374 V	378,5 V	380 V
19	54	376 V	380,2 V	381,6 V
20	57	378 V	381,5 V	383 V
21	60	380 V	382,8 V	384,4 V

The graph illustrating the time required to charge the capacitor to the voltage corresponding to 60 J of energy is presented in Figure 34 below.

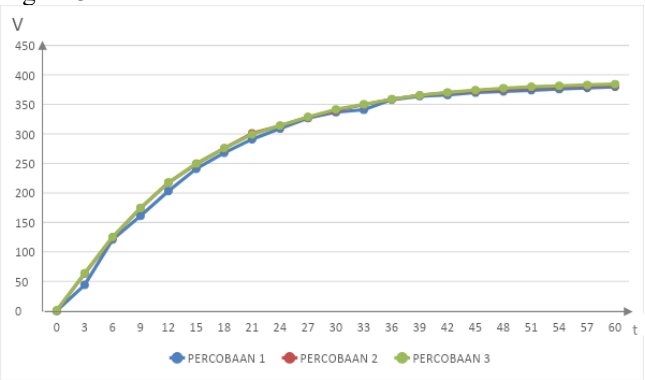

Fig. 34 Test results of 60 Joule capacitor charging time

Based on the aforementioned table, the capacitor charging time tests were conducted using an Avometer (multimeter). The results indicate that the charging time for the capacitor to reach 20 J was 12 seconds, while the maximum charging time to achieve 60 J was 60 seconds.

V. Conclusions and Suggestions

The conclusions derived from the research on the Design and Development of a Microcontroller-Based Portable Defibrillator, utilizing the Engineering Research method with four stages—data collection, planning, product development, and field testing—are as follows:

1. The development of a microcontroller-based portable defibrillator was achieved through the Engineering Research method, implemented in four stages: data collection, design, development, and testing.
2. The experimental results demonstrated successful capacitor voltage charging utilizing a primary 12 VDC power source, elevated to 400 VDC through a step-up module, to achieve precise target energy levels of 20 J, 30 J, 40 J, 50 J, and 60 J. Based on three independent measurements conducted for each energy setting, the average performance metrics revealed a progressive increase in voltage alongside varying error margins and charging efficiencies. Specifically, for the 20 J setting, an average voltage of 231.8 V was recorded with a minimal error margin of 0.8% and a high charging efficiency of 99.2%. The 30 J configuration yielded an average voltage of 284.2 V, accompanied by a slightly elevated error margin of 0.96% and an efficiency of 99.04%. At 40 J, the average voltage reached 332.6 V, though with a increased error margin of 3.7% and a corresponding efficiency of 96.3%. Notably, the 50 J energy level exhibited an average voltage of 365.7 V, achieving an exceptionally low error margin of 0.28% and the highest efficiency of 99.72%. Conversely, the 60 J setting resulted in an average voltage of 373.6 V but was marked by a significant error margin of 12.6% and a reduced efficiency of 87.4%, indicating potential limitations in the system's performance at higher energy demands. These findings underscore the system's robustness and precision for energy deliveries up to 50 J, while highlighting critical challenges that necessitate further optimization for applications requiring 60 J outputs.

Following the development and testing of the microcontroller-based simple defibrillator prototype, the researchers propose the following recommendations for future work:

1. The portable microcontroller-based defibrillator system can be further enhanced by expanding its energy delivery range to higher joule levels, enabling maximal energy adjustment capabilities for broader clinical applications.
2. The RC circuit design should incorporate additional components, specifically inductors, to improve patient safety by mitigating current transients and optimizing waveform characteristics.

REFERENCES

[1] Arios, R. R. (2020). *Em.diii.20.24 simulasi pengaturan energi pada defibrillator berbasis arduino nano*. (in bahasa)

[2] Asita Panjaitan, W. D. (2019). *Analisis tingkat keakurasian defibrillator di rumah sakit a*. (in bahasa)

[3] Dabukke, H. (2020). *Analisis kalibrasi akurasi energi pada defibrillator philips efficia dfm100*. *5*(November). (in bahasa)

[4] Dewi, D. A. M. S. (2017). Terapi fibrilasi. *Bagian Anestesi Dan Reanimasi Rumah Sakit Umum Pusat Sanglah Fakultas Kedokteran Universitas Udayana 2017*, 1–19. (in bahasa)

[5] Diah Ika Putri, M., Ma'arif, A., & Dwi Puriyanto, R. (2022). Pengendali Kecepatan Sudut Motor DC Menggunakan Kontrol PID dan Tuning Ziegler Nichols. *Techno (Jurnal Fakultas Teknik, Universitas Muhammadiyah Purwokerto)*, *23*(1). https://doi.org/10.30595/techno.v23i1.10773. (in bahasa)

[6] Dwi Astuti, M. (2019). Simulasi Otomatisasi Pengaturan Tegangan Berdasrakan Tebal Torax Pada Pesawat Rontgen Condensator Discharge. *Simulasi Otomatisasi Pengaturan Tegangan Berdasrakan Tebal Torax Pada Pesawat Rontgen Condensator Discharge*. (in bahasa)

[7] Halliday, Resnick, & Walker. (2011). Fundamentals of Physics-Halliday & Resnick. *Antimicrobial Agents and Chemotherapy*, *53*(12), 160. www.wileyplus.com

[8] Iqbal, M., Irianto, B. G., & Yulianto, E. (2020). Rancang Bangun Defibrilator dengan Joule kecil (Sinkron dan Asinkron). *Teknokes*, *13*(2), 68–74. (in bahasa)

[9] Joko, Y., Widodo, H., Elektro, J. T., Sains, F., Teknologi, D. A. N., & Dharma, U. S. (2017). *Tugas Akhir Charger Baterai Li-Po 3 Sel Menggunakan Flyback Konverter Dengan Masukan 220 Vac Final Project Charger Battery Li-Po 3 Cell Using Flyback Converter With 220 Vac Input*. (in bahasa)

[10] Kementrian Sekretariat Negeri Republik Indonesia. (2022). Instruksi Presiden Republik Indonesia Nomor 2 Tahun 2022 tentang percepatan peningkatan penggunaan produk dalam negeri dan produk usaha mikro, usaha kecil, dan koperasi dalam rangka menyukseskan gerakan nasional bangga buatan indonesia pada pelaksanaan pe. 132539. (in bahasa)

[11] Kurniawan, F. (2018). Pengembangan Model Boost-Buck untuk Mempertinggi Stabilitas Tegangan Keluaran Konverter DC-ke-DC. *Jurnal EECCIS*, *12*(2), 98–103. (in bahasa)

[12] Muhajirin, M., & Ashari, A. (2018). Perancangan Sistem Pengukur Detak Jantung Menggunakan Arduino Dengan Tampilan Personal Computer. *Inspiration : Jurnal Teknologi Informasi Dan Komunikasi*, *8*(1). https://doi.org/10.35585/inspir.v8i2.2458. (in bahasa)

[13] Nurpauzi, I., Studi, P., Elektronika, P. T., Teknik, F., & Jakarta, U. N. (2022). *SKRIPSI Rancang Bangun Sistem Solar Charger Controller Dengan Baterai Li-Ion Pada Mobil Listrik UNJ Berbasis Mikrokontroller dan IoT*. (in bahasa)

[14] Ogata, K. (2017). Modern control engineering. In *Modern Control Engineering*. https://doi.org/10.1201/9781315214573

[15] Perkins, W. J. (1968). Biomedical instrumentation. In *Journal of Physics E: Scientific Instruments* (Vol. 1, Issue 8). https://doi.org/10.1088/0022-3735/1/8/302

[16] Pratama, R. P. (2017). APLIKASI WEBSEaRVER ESP8266 UNTUK PENGENDALI PERALATAN LISTRIK. *INVOTEK: Jurnal Inovasi Vokasional Dan Teknologi*, *17*(2), 39–44. https://doi.org/10.24036/invotek.v17i2.87. (in bahasa)

[17] Saka Gilap Asa, P., Priyambodo, S., & Subandi. (2016). Sistem Pembelajaran Kontrol PID (Proporsional Integral Derivatif) Pada Pengatur Kecepatan Motor DC. *Jurnal Elektrikal*, *3*(1), 72–77. https://ejournal.akprind.ac.id/index.php/elektrikal/article/view/2483. (in bahasa)

[18] Setya, W. (2017). Karakteristik Rangkaian Ekivalen Dioda Blend Organik P3Ot : Pcbm. *Journal of Teaching and Learning Physics*, *2*(2), 7–12. https://doi.org/10.15575/jotalp.v2i2.6568. (in bahasa)

[19] Siagian, W. (2020). Analisis Prinsip Kerja Proses Charge Dan Discharge Pada Capasitor Dengan Rangkaian Rc. *Jurnal Ilmiah Simantek*, *4*(2), 44–53. (in bahasa)

[20] Sukma, I., Hidayat, S. W., & Ardiatna, W. (2017). the Effect of Inductor Resistance on Defibrillation Energy From Electrocardiograph Endurance Test System. *Widyariset*, *3*(1), 1. https://doi.org/10.14203/widyariset.3.1.2017.1-8

[21] Yusra Pintaningrum, Y. (2021). Fibrilasi Ventrikel: Mengenali Awitan Hingga Tatalaksana. *Unram Medical Journal*, *10*(2), 494–501. https://doi.org/10.29303/jku.v10i2.558. (in bahasa)